Chinese Journal of Catalysis 37 (2016) 1539–1548

available at www.sciencedirect.com

ScienceDirect

journal homepage: www.elsevier.com/locate/chnjc

Article

Enantioselective epoxidation of unfunctionalized olefins by Jacobsen's catalyst immobilized on amino-modified ZnPS-PVPA

Jing Huang [a,b,*], Yan luo [c], Jiali Cai [d]

[a] *Research Center for Advanced Computation, Xihua University; College of Science, Xihua University, Chengdu 610039, Sichuan, China*
[b] *Institute for Clean Energy & Advanced Materials, Southwest University, Chongqing 400715, China*
[c] *College of Materials and Chemical Engineering, Chongqing University of Arts and Science, Chongqing 402160, China*
[d] *College of Rongchang, Southwest University, Chongqing 402460, China*

ARTICLE INFO

Article history:
Received 28 April 2016
Accepted 28 May 2016
Published 5 September 2016

Keywords:
Chiral salen Mn(III)
Aryldiamine
Alkyldiamine
Asymmetric epoxidation of olefins
Zinc poly (styrene-phenyl-vinylphosphonate)-phosphate

ABSTRACT

Catalytic asymmetric epoxidation of alkenes is a powerful method for the synthesis of chiral organic compounds. A recyclable chiral Jacobsen's catalyst immobilized on ZnPS-PVPA on diamines gave high catalytic activity (conversion > 99%, ee > 99%) in the asymmetric epoxidations of unfunctionalized olefins. The synergistic effect of the support ZnPS-PVPA and the linkage as well as chiral salen Mn center contributed to the chirality of the product. The stability (recycled nine times) and the ease of use in large scale reactions (200 times scale) indicated a catalyst useful for industrial use.

1. Introduction

High atomic efficiency for waste free processes is an important goal in asymmetric catalysis in the chirality economy [1,2]. High enantioselectivity has been achieved with homogeneous catalysts, but their separation, recovery, and reuse remain arduous [3–7]. Clearly, heterogeneous catalysts with high enantioselectivity would be an important development for applications in industrial and high throughput organic chemistry [8–10].

The catalytic epoxidation of olefins is a subject of growing interest in the production of chemicals and fine chemicals because epoxides are the key starting materials for a wide variety of products [11,12]. Much effort has been made to develop new active and selective epoxidation catalysts for the processes with the aim to eliminate byproducts. Jacobsen epoxidation [13] has emerged as a powerful method for the asymmetric oxidation of unfunctionalized olefins. It is catalyzed by structurally simple Mn(III)-salen complexes and has been optimized in terms of the catalyst structure and choice of stoichiometric oxidants and other additives. Recently, various methods have been employed to heterogenize Mn-salen complexes on nanoporous materials [14–24].

We have worked to immobilize Jacobsen's catalyst on a se-

* Corresponding author. Tel: +86-18203070132; Fax: +86-28-87720037; E-mail: hj41012@163.com
This work was supported by the Fundamental Research Funds for the Central Universities (XDJK2013C120), Xihua University Key Projects (Z1223321), Sichuan Province Applied Basic Research Projects (2013JY0090), Department of Education of Sichuan Province Projects (13ZB0030), Chongqing Special Funding for Postdoctoral (Xm2014028), Chongqing Postdoctoral Daily Fund (Rc201419), and Scientific and Technological Research Program of Chongqing Municipal Education Commission (KJ1501127).
DOI: 10.1016/S1872-2067(16)62489-0 | http://www.sciencedirect.com/science/journal/18722067 | Chin. J. Catal., Vol. 37, No. 9, September 2016

ries of hybrid materials, such as zirconium oligostyrenylphosphonate-phosphate (ZSPP) and zirconium poly(styrene-phenylvinylphosphonate)-phosphate (ZPS-PVPA) and zinc poly(styrene-phenylvinylphosphonate)-phosphate (ZnPS-PVPA) and calcium poly(styrene-phenylvinylphos-phonate)-phosphate (CaPS-PVPA). The heterogeneous chiral salen Mn(III) catalysts showed superior performance in the asymmetric epoxidation of unfunctionalized olefins[25–32].

We have the general goals of designing and synthesizing new chiral catalysts in an efficient and economical manner on a large scale. In this work, we used Jacobsen's catalyst anchored on amino-modified ZnPS-PVPA for the asymmetric epoxidations of unfunctionalized olefins. To investigate the effects of the diamines as the linkers on the morphology and disposition of the catalysts, we introduced alkyl diamines and aryl diamines into the catalysts. The immediate goals of our studies were to evaluate the effect of a distribution of chiral ligands on the enantioselectivity of alkene epoxidation and to determine the extent to which the catalyst can be recycled for repeated use as well as to investigate the catalysts in large scale reactions. The results of these efforts are described here.

2. Experimental

2.1. Materials and instruments

All chemicals and reagents were analytical grade and used as received. All solvents were further purified before use. The chiral salen ligand and chiral homogeneous catalyst salen Mn(III) were synthesized according to standard literature procedures [33], and were identified by the analysis and comparison of the IR spectra with the literature [34].

FT-IR spectra were recorded using KBr pellets and a Bruker RFS100/S spectrophotometer (USA). The diffuse reflectance UV-Vis spectra of the solid samples were recorded on a spectrophotometer with an integrating sphere using $BaSO_4$ as standard. ^1H NMR and ^{31}P NMR were performed on an AV-300 NMR instrument at ambient temperature at 300 and 121 MHz, respectively. All of the chemical shifts were reported downfield in ppm relative to the hydrogen and phosphorus resonance of TMS and 85% H_3PO_4, respectively. Number and weight average molecular weights (M_n and M_w) and polydispersity (M_w/M_n) were estimated using a Waters1515 gel permeation chromatograph (GPC; against polystyrene standards) using THF as eluent (1.0 mL/min) at 35 °C. X-ray photoelectron spectrum was recorded on ESCALab 250 instrument. The interlayer spacings were obtained using a DX-1000 automated X-ray power diffractometer, using Cu K_α radiation and an internal silicon powder standard with all samples. The patterns were measured between 3.00° and 80.00° with a step size of 0.02°/min. The X-ray tube settings were 36 kV and 20 mA. C, H and N elemental analysis was obtained using an EATM 1112 automatic elemental analyzer instrument (Thermo, USA). TG analyses were performed on an SBTQ600 thermal analyzer (USA) with the heating rate of 20 °C/min from 25 to 1000 °C under flowing N_2 (100 mL/min). The Mn contents of the catalysts were determined by a TAS-986G (Pgeneral, China) atomic absorption spectroscopy. SEM was performed on a KYKY-EM 3200 (KYKY, China) microscope. TEM was obtained on a TECNAI10 (PHILIPS, Holland) apparatus. Nitrogen adsorption isotherms were measured at –196 °C on a 3H-2000I (Huihaihong, China) volumetric adsorption analyzer with the BET method. The racemic epoxides were prepared by the epoxidation of the corresponding olefins by 3-chloroperbenzoic acid in CH_2Cl_2 and confirmed by NMR (Bruker AV-300). Gas chromatography (GC) was calibrated with the samples of *n*-nonane, olefins and the corresponding racemic epoxides. The conversion (with *n*-nonane as internal standard) and ee value were obtained by GC with a Shimadzu GC2010 (Japan) instrument equipped with a chiral column (HP19091G-B213, 30 m × 30 m × 0.32 mm × 0.25 μm) and FID detector using injector 230 °C, detector 230 °C. Ultrapure nitrogen was used as the carrier (rate 34 mL/min) with a carrier pressure of 39.1 kPa and the injection port temperature was set at 230 °C.

2.2. Synthesis of the catalysts (Scheme 1)

2.2.1. Synthesis of styrene-phenylvinylphosphonic acid

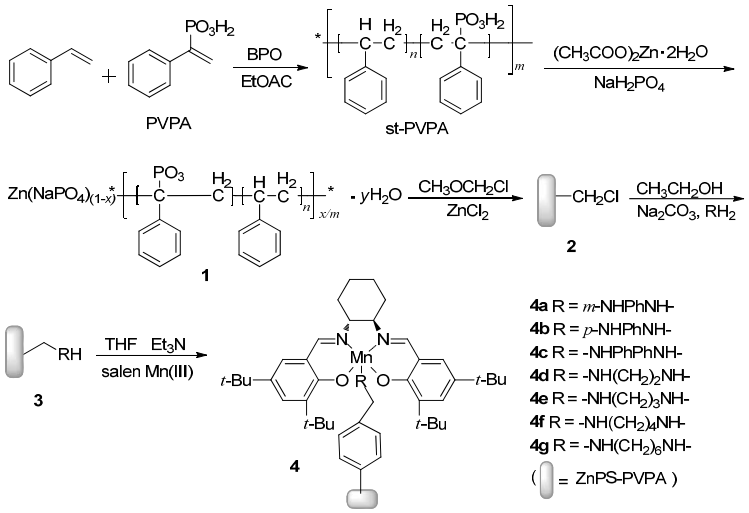

Scheme 1. Synthesis of the heterogeneous catalysts.

copolymer (PS-PVPA)

1-Phenylvinyl phosphonic acid (PVPA) was synthesized according to the literature [35]. Its structure was confirmed by ^{1}H NMR, ^{31}P NMR and FT-IR. ^{1}H NMR ($CDCl_3$): δ = 6.06 (d, 1H), 6.23 (d, 1H), 7.26–7.33 (m, 3H), 7.48 (m, 2H). ^{31}P NMR (CD_3OD): δ = 15.9. IR (KBr): ν = 2710, 2240, 1500, 1200, 1040, 950, 780, 720, 700 cm^{-1}. Yield: 90%.

1-Phenylvinyl phosphonic acid (4 g, 21.7 mmol), styrene (20 mL, 173.9 mmol), ethyl acetate (150 mL) and benzoyl peroxide (BPO, 1.0 g, 4.7 mmol) were used for the preparation of PS-PVPA (7.52 g in 47% yield) as reported in the literature [29]. GPC: M_n = 39700, m = 38.3, n = 8.2, M_w/M_n = 2.

*2.2.2. Synthesis of zinc poly(styrenephenylvinylphosphonate)-phosphate (ZnPS-PVPA, **1**)*

PS-PVPA (1.0 g, 1 mmol), sodium dihydrogen phosphate (0.62 g, 4 mmol), zinc acetate (1.1 g, 5 mmol) and Et_3N (0.68 g, 6.7 mmol) were used for the synthesis of ZnPS-PVPA according to the literature [30]. IR (KBr): ν = 3059, 3028, 2923 (CH), 1686, 1493, 1453, 756, 698 (–C_6H_5), 1027 (P=O) cm^{-1}. Found: C 58.08%, H 4.97%; Calc. for $C_{72}H_{73}O_{11}P_3Na_2Zn_3$: C 59.71%, H 5.04%.

*2.2.3. Synthesis of chloromethyl-zinc poly (styrene-phenylvinyl-phosphonate)-phosphate (ZnCMPS-PVPA, **2**)*

Chloromethyl methyl ether (9.3 mL), anhydrous zinc chloride (3.32 g, 24.34 mmol) and ZnPS-PVPA (5.0 g, 3.4 mmol) were mixed in 40 mL chloroform and stirred at 40 °C for 10 h. Then, sodium carbonate saturated solution was added to neutralize the mixture. The solvent was evaporated under reduced pressure, followed by filtering, washing and drying in vacuo to obtain ZnCMPS-PVPA (5.84 g, 90.1%). IR (KBr): ν = 3026, 2925 (CH), 2341(O=P–OH), 1650, 1542, 1510, 1493 (–C_6H_5), 1267 (P=O), 700 (C–Cl) cm^{-1}. Found: C 51.16%, H 4.09%; Calc. for $C_{80}H_{81}O_{11}P_3Cl_8Na_2Zn_3$: C 52.31%, H 4.41%.

*2.2.4. Synthesis of aminomethyl-zinc poly(styrene-phenylvinyl-phosphonate)-phosphate (ZnAMPS-PVPA, **3**)*

A proportional amount of *m*-phenylenediamine was blended with **2** (1 g), Na_2CO_3 (1.06 g, 0.01 mol), and alcohol 50 mL (the molar ratio of alkyl diamine to chlorine element in **2** is 5:1). After the mixture was stirred and kept at 70 °C for 12 h, the product **3a** was filtered, washed, and dried in vacuo. The product **3(b–g)** was obtained by a similar course. The products were abbreviated as **3(a–g)**. **3a**, Found: C 62.16%, H 5.21%, N 9.16%; Calc. for $C_{128}H_{137}N_{16}O_{11}P_3Na_2Zn_3$: C 63.81%, H 5.69%, N 9.31%. **3b**, Found: C 61.15%, H 5.02%, N 9.05%; Calc. for $C_{128}H_{137}N_{16}O_{11}P_3Na_2Zn_3$: C 63.81%, H 5.69%, N 9.31%. **3c**, Found: C 69.16%, H 5.45%, N 7.26%; Calc. for $C_{176}H_{169}N_{16}O_{11}P_3Na_2Zn_3$: C 70.05%, H 5.61%, N 7.43%. **3d**, Found: C 57.36%, H 6.85%, N 8.93%; Calc. for $C_{92}H_{133}N_{12}O_{11}P_3Na_2Zn_3$: C 57.58%, H 6.93%, N 9.01%. **3e**, Found: C 59.01%, H 7.23%, N 8.45%; Calc. for $C_{100}H_{149}N_{12}O_{11}P_3Na_2Zn_3$: C 59.12%, H 7.33%, N 8.52%. **3f**, Found: C 60.27%, H 7.58%, N 7.95%; Calc. for $C_{108}H_{165}N_{12}O_{11}P_3Na_2Zn_3$: C 60.51%, H 7.69%, N 8.08%. **3g**, Found: C 62.73%, H 8.25%, N 7.26%; Calc. for $C_{124}H_{197}N_{12}O_{11}P_3Na_2Zn_3$: C 62.89%, H 8.32%, N 7.31%.

*2.3. Synthesis of chiral salen Mn(III) catalyst anchored on ZnAMPS-PVPA (**4**)*

Chiral salen Mn(III) (4 mmol) in 10 mL of THF was added dropwise to the solution of **3a** (0.5 g) pre-swelled in THF for 30 min and Et_3N (5 mmol) with stirring. Then the mixture was refluxed for 10 h, followed by neutralizing and evaporating. The dark brown powder **4a** was obtained by filtration and washing. Samples **4**(**b–c**) were obtained by the same process. For samples **4**(**d–g**), chiral salen Mn(III) (4 mmol) in 10 mL of THF was added dropwise to the solution of **3a** (0.5 g) pre-swelled in THF for 30 min and Et_3N (5 mmol) with stirring. Then the mixture was refluxed for 10 h. After cooling down, the solution was neutralized and the solvent was evaporated. The dark brown powder **4a** was obtained by filtration and washed thoroughly with CH_2Cl_2 and deionized water respectively until no Mn could be detected by AAS. **4a**, Found: C 70.16%, H 7.21%, N 3.05%; Calc. for $C_{416}H_{545}N_{32}O_{27}P_3Na_2Zn_3Mn_8$: C 71.65%, H 7.82%, N 3.22%. **4b**, Found: C 69.15%, H 7.01%, N 2.91%; Calc. for $C_{416}H_{545}N_{32}O_{27}P_3Na_2Zn_3Mn_8$: C 71.65%, H 7.82%, N 3.22%. **4c**, Found: C 70.17%, H 7.25%, N 5.26%; Calc. for $C_{464}H_{577}N_{32}O_{27}P_3Na_2Zn_3Mn_8$: C 71.39%, H 7.40%, N 5.74%. **4d**, Found: C 67.91%, H 7.93%, N 5.86%; $C_{380}H_{541}N_{28}O_{27}P_3Na_2Zn_3Mn_8$: C 68.03%, H 8.07%, N 5.93%. **4e**, Found: C 68.26%, H 8.06%, N 5.74%; Calc. for $C_{388}H_{557}N_{28}O_{27}P_3Na_2Zn_3Mn_8$: C 68.32%, H 8.17%, N 5.83%. **4f**, Found: C 68.52%, H 8.16%, N 5.62%; Calc. for $C_{396}H_{573}N_{28}O_{27}P_3Na_2Zn_3Mn_8$: C 68.60%, H 8.27%, N 5.73%. **4g**, Found: C 69.02%, H 8.37%, N 5.48%; Calc. for $C_{412}H_{605}N_{28}O_{27}P_3Na_2Zn_3Mn_8$: C 69.14%, H 8.46%, N 5.55%.

2.4. Synthesis of alkyldiamino-modified chiral salen Mn(III) (Scheme 2)

p-phenylenediamine (20 mmol) and Na_2CO_3 (0.848 g, 8 mmol) were blended with benzyl bromide at 70 °C for 6 h to gain compound **5a**. The subsequent procedure was similar to that used for the heterogeneous catalyst (in Section 2.3). **6a**, IR

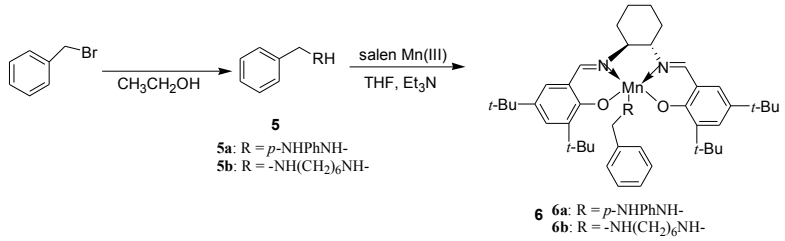

Scheme 2. Synthesis of the homogeneous catalysts.

(KBr): ν = 1650, 1542, 1510, 1493 (–C_6H_5), 1140 (–NH_2), 3415, 1617 (–NH–), 1639 (–C=N) cm^{-1}. Found: C 73.68%, H 8.03%, N 6.95%; Calc. for $C_{42}H_{59}N_4O_2Mn$: C 73.87%, H 8.17%, N 7.04%. **6b**, IR (KBr): ν = 3410, 1620 (–NH–), 3024, 2927 (CH), 2339 (O=P–OH), 1651, 1543, 1513, 1492 (–C_6H_5), 1639 (–C=N), 1262 (P=O) cm^{-1}; Found: C 72.85%, H 8.91%, N 6.92%; Calc. for $C_{48}H_{71}N_4O_2Mn$: C 72.91%, H 8.99%, N 7.09 %.

2.5. Asymmetric epoxidation

2.5.1. Using m-CPBA as oxidant

For *m*-CPBA/NMO, the activity of the prepared catalysts was tested with alkene (1 mmol), *n*-nonane (internal standard, 1 mmol), NMO (5 mmol), homogeneous (5 mol%) or heterogeneous salen Mn(III) catalysts (5 mol%) and *m*-CPBA (2 mmol) for the epoxidation of unfunctionalized olefins in CH_2Cl_2. After the reaction, Na_2CO_3 (2 mL, 1.0 mol/L) was added to quench the reaction.

2.5.2. Using $NaIO_4$ as oxidant

For the $NaIO_4$/imidazole system, the reaction was carried out with alkene (1 mmol), $NaIO_4$ (2 mmol) and the catalyst (5 mol%) in a mixture of acetonitrile : water = 2:1.

2.6. Reusability of the catalyst

In a typical recycling test, an equal volume of hexane was added to the mixture after the reaction. Subsequently, the organic phase was separated, followed by washing and drying. The recovered catalyst was weighed and reused in the next run. In all runs, the same proportion of substrate-to-catalyst and solvent-to-catalyst was retained.

2.7. General procedure for the large scale asymmetric epoxidation reaction

A solution of catalyst **4d** (2.5 mmol), *n*-nonane (50 mmol) and α-methylstyrene (50 mmol) in CH_2Cl_2 (150 mL) at –40 °C was stirred for 30 min. Then, *m*-CPBA (100 mmol) was added to the solution step by step. After Na_2CO_3 (100 mL, 1.0 mol/L) was added to quench the reaction, the organic layer was dried over sodium sulfate. The conversions and ee values of the epoxide were determined by GC.

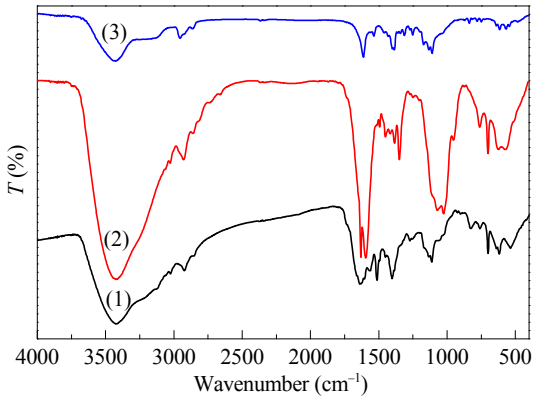

Fig. 1. FT-IR spectra of (1) **4b**, (2) **4g** and (3) Jacobsen's catalyst.

3. Results and discussion

3.1. Characterizations of the heterogeneous chiral catalysts

3.1.1. IR spectroscopy and UV-Vis spectroscopy

Catalysts **4**(**a**–**g**) and Jacobsen's catalyst have the same band at 1638 cm^{-1} (Fig. 1) due to the vibration of the imine group. The azomethene (C=N) stretching band was in the vicinity of 1617 cm^{-1} for Jacobsen's catalyst and the supported catalysts. The band at 3408 cm^{-1} was observed for the catalysts, which was assigned to the stretching vibration of N–H groups. The stretching vibration at 1030 cm^{-1} which was assigned to the vibrations of the phosphonate and phosphate in the support ZnPS-PVPA was obviously weakened by the electronic structure changes of the host-guest interaction. The common prominent bands at 1145, 1089, and 986 cm^{-1} were assigned to the R-PO_3^{2-} phosphonate stretching vibrations. The phosphonate and phosphate stretching vibrations contributed to the adsorption at 1201, 1144, and 1077 cm^{-1}.

In the UV-Vis spectra (Fig. 2), the band at 335 nm can be attributed to the charge transfer transition of the salen ligand. The band at 433 nm was due to the ligand-to-metal charge transfer transition. The band at 510 nm was assigned to the *d*–*d* transition of salen Mn(III) complex. Moreover, the interaction

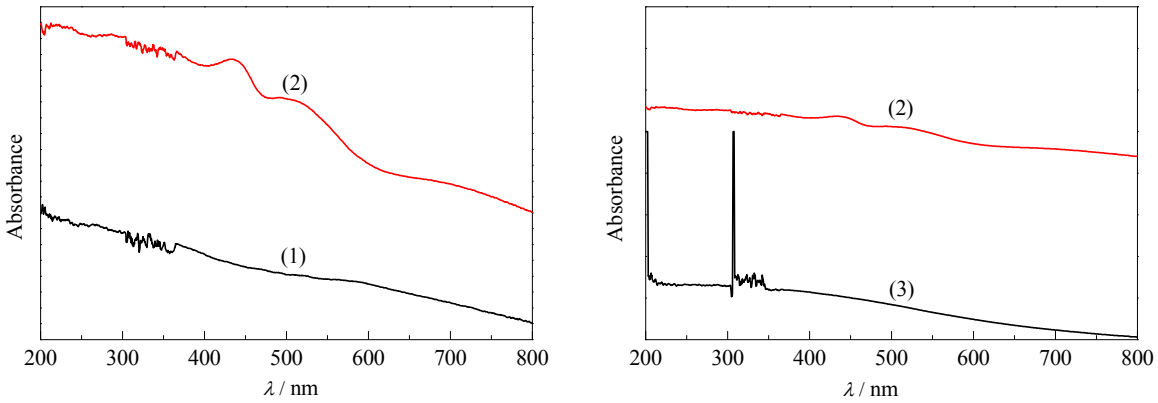

Fig. 2. Solid reflectance UV-Vis spectra of (1) **4b**, (2) Jacobsen's catalyst and (3) **4g**.

between the salen Mn(III) complex and the amino-modified ZnPS-PVPA contributed to the blue shifts of Jacobsen's catalyst and the supported catalysts.

3.1.2. *Thermal gravimetric analysis and powder XRD*

For catalyst **4b** (Fig. 3(a)), the initial mass loss was 3.38% below 200 °C due to the loss of surface-bound and intercalated water. Subsequently, the organic moieties decomposed with 69.32% mass loss in the temperature range of 200–850 °C. For catalyst **4g** (Fig. 3(b)), a similar mass loss procedure occurred with an initial 3.5% mass loss below 180 °C and then 56.8% mass loss for the decomposition of the organic moieties in the range of 180–700 °C. Notably, both catalysts **4b** and **4g** still maintained superior stability below 180 °C, which indicated that the heterogeneous catalysts can be utilized in asymmetric epoxidation.

Compared with ZnPS-PVPA (Fig. 4), many crystalline peaks have disappeared or were diminished for catalysts **4b** and **4g** upon the immobilization of Jacobsen's catalyst. For catalyst **4b**, the intensity of the peaks at 2.02°, 25.4° and 42.16° decreased with a small shift toward lower 2θ values, which confirmed that the mesoporous structure of the parent support remained intact after the modification with aryl diamine. Some peaks in the XRD pattern of the catalyst were relatively reinforced as the other peaks weakened. A similar phenomenon occurred with catalyst **4g**. In addition, the interlayer distance of catalyst **4b** (4.33 ± 0.02 nm) was nearly twice that of ZnPS-PVPA (2.1 ± 0.13 nm) owing to the introduction of Jacobsen's catalyst on the *p*-phenylenediamine that made the zinc layer stretch. For catalyst **4g**, the interlayer distance (0.237 ± 0.01 nm) was instead narrower than that of ZnPS-PVPA (2.1 ± 0.13 nm) by virtue of Jacobsen's catalyst being anchored on ZnPS-PVPA through 1,6-diaminohexane. In the configuration of catalysts **4b** and **4g**, the difference lies in the rigid linker for **4b** and the flexible linker for **4g**. In essence, the mode of the immobilization of Jacobsen's catalyst and the corresponding microenvironment contributed to the phenomenon.

3.1.3. *N_2 adsorption isotherm*

As described in Fig. 5(a), catalyst **4b** showed a distribution of pore size of 2–8 nm and a characteristic Type V isotherm. For catalyst **4g** (Fig. 5(b)), the N_2 adsorption isotherm was characteristically Type V with a distinct hysteresis loop (Type H_1). The pore diameters varied from 1 to 18 nm, and a small amount below 2 nm and a few over 50 nm in diameter. The textural parameters calculated from the N_2 adsorption isotherms and Mn content of the immobilized catalysts were shown in Table 1.

For catalyst **4b**, after the chloromethylation and arylamination, obvious increases in the BET surface area (**1**, **2** and **3b**, from 4.9 to 36.9 and to 42.5 m^2/g) and pore volume (**1**, **2** and

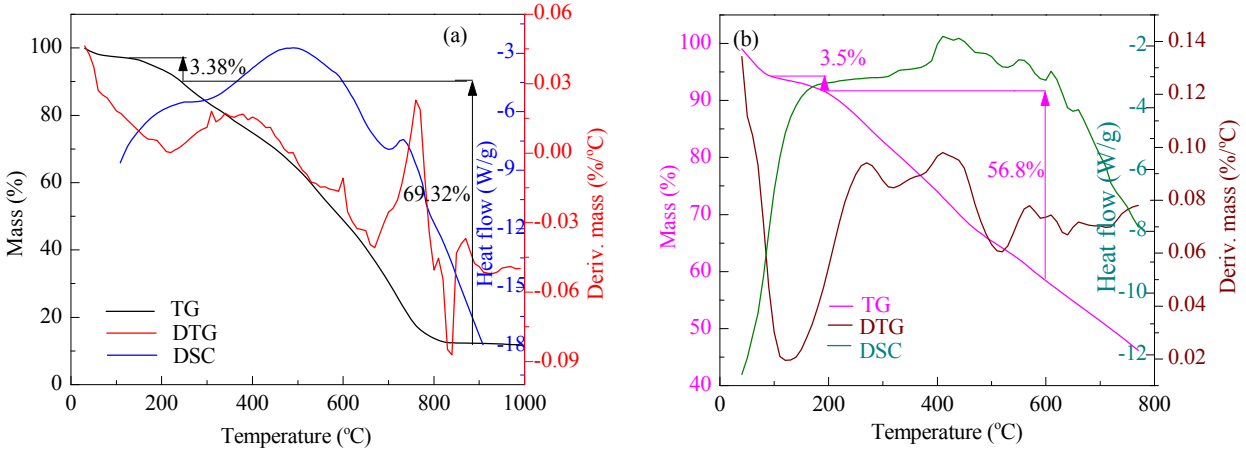

Fig. 3. TG curves of catalysts (a) **4b** and (b) **4g**.

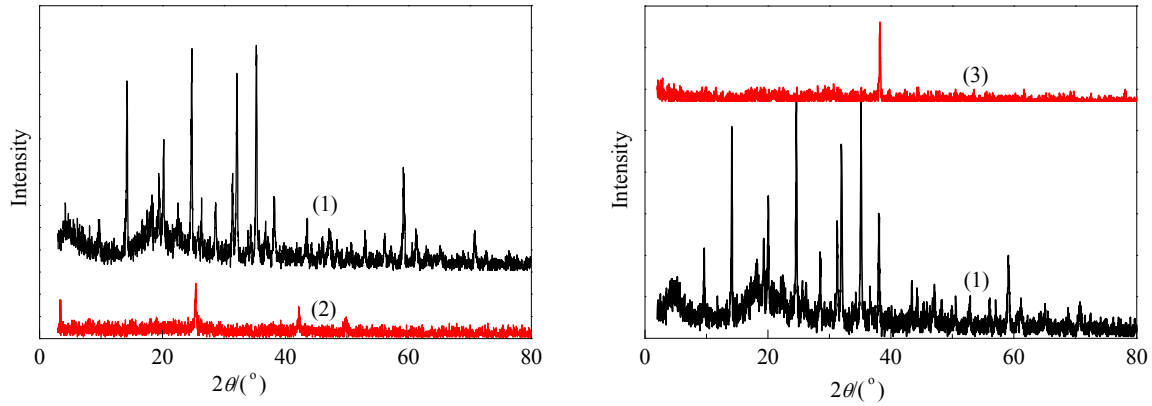

Fig. 4. XRD patterns of (1) ZnPS-PVPA, (2) catalyst **4b** and (3) catalyst **4g**.

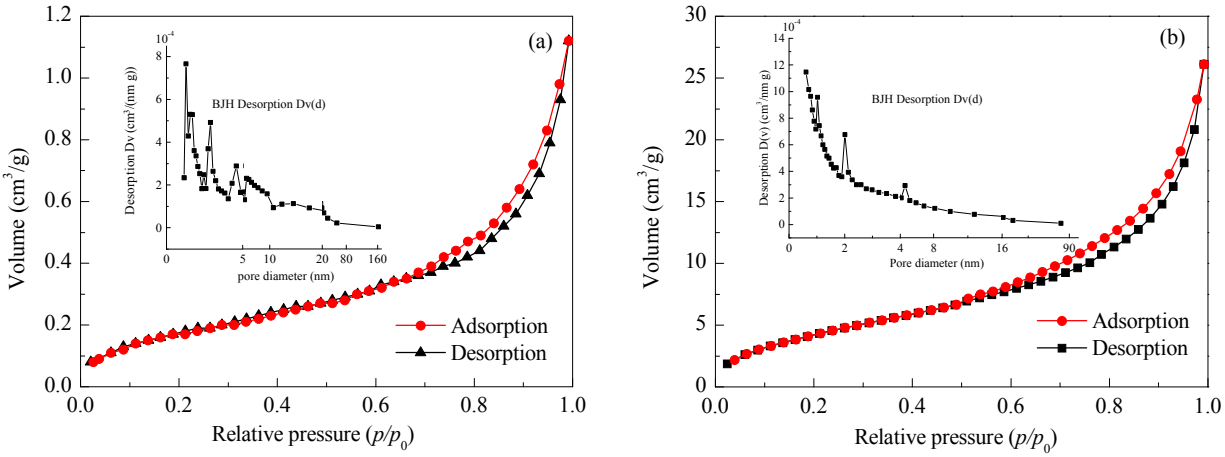

Fig. 5. N_2 adsorption isotherms and pore distribution of catalysts (a) **4b** and (b) **4g**.

Table 1
Physical properties of 1, 2, 3b, 4b and 4g.

Sample	Surface area (m^2/g)	Pore volume (cm^3/g)	Average pore diameter (nm)	Mn content (mmol/g)
1	4.9	0.013	3.5	—
2	36.9	0.1882	10.21	—
3b	42.5	0.242	11.39	—
4b	31.66	0.0543	1.56	0.72
4g	28.02	0.04442	0.61	0.73

3b, from 0.013 to 0.1882 and to 0.242 cm^3/g) and pore diameter (**1**, **2** and **3b**, from 3.5 to 10.21 and to 11.39 nm) were observed. In contrast, upon the immobilization of chiral salen Mn(III) onto ZnPS-PVPA, decreases were seen in the BET surface area (**3b** and **4b**, from 42.5 to 31.66 m^2/g), pore volume (**3b** and **4b**, from 0.242 to 0.0543 cm^3/g) and pore diameter (**3b** and **4b**, from 11.39 to 1.56 nm). For catalyst **4g**, owing to the immobilization of Jacobsen's catalyst, the textural parameters similarly showed a decrease in BET surface area (**2** and **4g**, from 36.9 to 28.02 m^2/g), pore volume (**2** and **4g**, from 0.1882 to 0.04442 cm^3/g) and pore diameter (**2** and **4g**, from 10.21 to 0.61 nm). From these facts, it can be deduced that two forms of the immobilization of Jacobsen's catalyst existed: inner type and outer type.

3.1.4. *Analysis of surface morphology*

From the SEM photographs (Fig. 6), catalysts **4b** and **4g** have a similar loose amorphous configuration, which confirmed that the morphology of the catalysts did not depend on the linker. Moreover, the morphology of **4b** and **4g** was much transformed versus ZnPS-PVPA (smooth anomalous structure), which was different from most of the results reported [25–27] such as the immobilized chiral salen Mn(III) on ZPS-PVPA. Simultaneously, many small caves and channels with irregular shapes also were present. The amorphous morphology and porous structure of the catalysts together would increase the surface area (ZnPS-PVPA, **4b**, and **4g**; 4.9, 31.66 and 28.02 m^2/g) and helped substrates onto the catalytic active sites.

As described in Fig. 7, both the catalysts **4b** and **4g** showed a loose configuration. Meanwhile, channels, holes and caves also

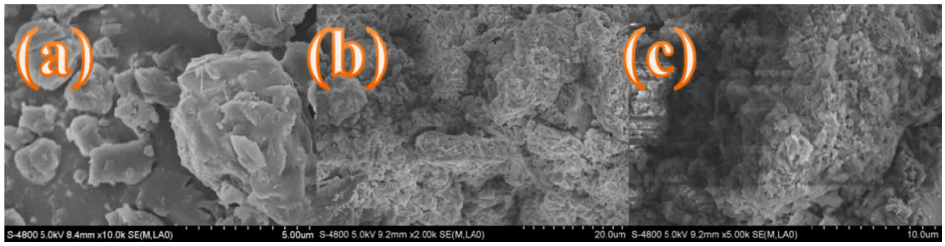

Fig. 6. SEM photographs of (a) ZnPS-PVPA, (b) catalyst **4b** and (c) catalyst **4g**.

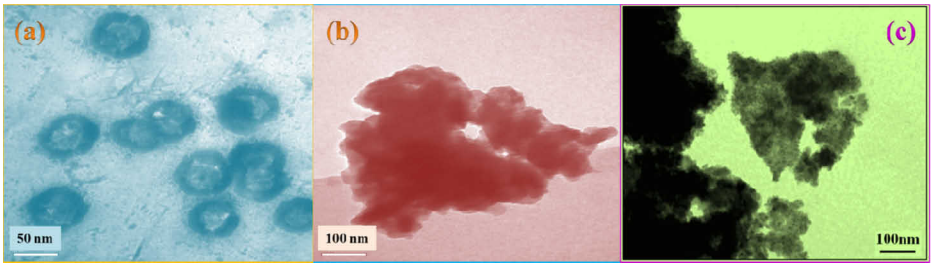

Fig. 7. TEM photographs of (a) ZnPS-PVPA, (b) catalyst **4b** and (c) catalyst **4g**.

existed, which confirmed that the linkers hardly had an effect on the morphology. Notably, the TEM images of catalysts **4b** and **4g** were changed compared to that of ZnPS-PVPA which manifested a spheroid structure. Therefore, the special configuration of the catalysts helped the substrates get to the internal catalytic active sites easily and provided enough space for the asymmetric epoxidation of unfunctionalized olefins.

3.2. Catalytic epoxidation of unfunctionalized olefins

3.2.1. Effect of different oxidants

3.2.1.1. Oxidation system of m-CPBA/NMO

To investigate the control of the chirality of the product, the support ZnPS-PVPA and **3b** as well as homogeneous catalyst **6a** were utilized to epoxidize indene (Table 2). Low olefin enantio-excesses were obtained (ee = 0% in entry 17 and ee = 22.6% in entry 6), which indicated that both ZnPS-PVPA and the support **3b** were stereochemically inactive for the epoxidation of olefins. Meanwhile, the ee values increased from 54% to 83.7% (Jacobsen's and **6a**, entry 1 and entry 8) due to the modification of *p*-phenylenediamine and further increased to >99% (**6a** vs **4b**, entry 8 vs entry 3) upon the immobilizing on ZnPS-PVPA. In the asymmetric epoxidation of *α*-methylstyrene and styrene, similar observations were also taken. Based on these results, it was deduced that for the catalysts **4**(**a–c**), a synergistic effect of the support ZnPS-PVPA, linkage aryl diamine and chiral salen Mn center contributed to the chirality of the products.

For catalysts **4**(**d–g**), a similar synergism affected the enantioselectivity, which was also unrelated to the linkers. Upon the functionalization of alkyl diamine and immobilization, the ee values increased from 54% to 86.7% (entry 1 vs entry 15) and further up to 98% (entry 12).

3.2.1.2. Oxidation system of $NaIO_4$/imidazole

Table 2
Asymmetric epoxidation of α-methylstyrene and indene catalyzed by homogeneous and heterogeneous catalysts (**4**(**a–g**)) with *m*-CPBA/NMO [a] and $NaIO_4$/imidazole [b] as oxidant systems.

Entry	Substrate	Catalyst	Oxidant system	Time (h)	Conversion (%)	ee of (*S*)-form (%)	TOF [c] (10^{-4} s^{-1})
1	indene	Jacobsen's	*m*-CPBA/NMO	1	98	54	54.42
2	indene	**4a**	*m*-CPBA	1	80.5	94.5	44.72
3	indene	**4b**	*m*-CPBA	1	>99	>99	55.55
4	indene	**4c**	*m*-CPBA	1	86.4	92.3	48.00
5	indene	**4b**	*m*-CPBA/NMO	1	7.8	4.5	4.33
6	indene	**3b**	*m*-CPBA	1	>99	22.6	55.55
7	indene	**6a**	*m*-CPBA/NMO	1	91.2	25.5	50.66
8	indene	**6a**	*m*-CPBA	1	98.7	83.7	54.83
9	indene	**4d**	*m*-CPBA/NMO	1	80	81	44.44
10	indene	**4e**	*m*-CPBA/NMO	1	82	85	45.58
11	indene	**4f**	*m*-CPBA/NMO	1	92	92	51.09
12	indene	**4g**	*m*-CPBA/NMO	1	>99	98	54.99
13	indene	**4g**	*m*-CPBA	1	51	8	28.35
14	indene	**3g**	*m*-CPBA/NMO	1	>99	16.83	54.99
15	indene	**6b**	*m*-CPBA/NMO	1	89	86.7	49.44
16	indene	**6b**	*m*-CPBA	1	76	82.5	42.21
17	indene	ZnPS-PVPA	*m*-CPBA/NMO	1	>99	0	54.99
18	α-methylstyrene	Jacobsen's	$NaIO_4$/imidazole	5	>99	69	11.11
19	α-methylstyrene	**4a**	$NaIO_4$/imidazole	5	>99	>99	11.11
20	α-methylstyrene	**4b**	$NaIO_4$/imidazole	5	>99	>99	11.11
21	α-methylstyrene	**4c**	$NaIO_4$/imidazole	5	>99	>99	11.11
22	α-methylstyrene	**4b**	$NaIO_4$	5	>99	>99	11.11
23	α-methylstyrene	**6a**	$NaIO_4$/imidazole	5	>99	>99	11.11
24	α-methylstyrene	**6a**	$NaIO_4$	5	>99	>99	11.11
25	α-methylstyrene	**4d**	$NaIO_4$/imidazole	5	>99	>99	11.11
26	α-methylstyrene	**4e**	$NaIO_4$/imidazole	5	>99	>99	11.11
27	α-methylstyrene	**4f**	$NaIO_4$/imidazole	5	>99	>99	11.11
28	α-methylstyrene	**4g**	$NaIO_4$/imidazole	5	>99	>99	11.11
29	α-methylstyrene	**4g**	$NaIO_4$	5	>99	>99	11.11
30	α-methylstyrene	**6b**	$NaIO_4$/imidazole	5	86	82	9.65
31	α-methylstyrene	**6b**	$NaIO_4$	5	83	79	9.31

[a] Reactions were carried out at –20 °C in CH_2Cl_2 (3 mL) with indene (1 mmol), *n*-nonane (internal standard, 1 mmol), NMO (5 mmol), homogeneous (5 mol%) or heterogeneous salen Mn(III) catalysts (5 mol%) and *m*-CPBA (2 mmol). The conversion and the ee value were determined by GC with chiral capillary columns HP19 091G-B213, 30 m × 0.32 mm × 0.25 μm.
[b] Reactions conditions: alkene (1 mmol), $NaIO_4$ (2 mmol), catalyst (0.03 mmol), CH_3CN/H_2O (10 mL/5 mL).
[c] Turnover frequency calculated by [product]/[catalyst] × time.

For catalysts **4**(**a–c**), the catalytic activities were comparable to the homogeneous catalyst **6a** and Jacobsen's catalyst (ee, >99% vs >99% vs 69%; entries 19–21 vs entry 23 vs entry 18). The conversion and enantioselectivity of catalyst **4b** exceeded 95%, even >99%. From catalysts **4**(**d–g**), the catalytic dispositions remained superior to Jacobsen's catalyst and the homogenous catalyst **6b** (ee, **4**(**d–g**) vs Jacobsen's vs **6b**; >99% vs 69% vs 82%, entries 25–28 vs entry 18 vs entry 30). Apart from this, the ee values varied from 69% (Jacobsen's, entry 18) to 82% (**6b,** entry 30) through the modification of 1,6-hexanediamine, followed by increasing to >99% (**4g**, entry 28) upon the immobilization of catalyst **6b** on ZnPS-PVPA. That is, the combined effects of ZnPS-PVPA and the linker as well as chiral ligand contributed to the superior activity in $NaIO_4$/imidazole.

3.2.2. *Effect of the linkage*

According to *m*-CPBA/NMO, catalyst **4b** showed higher activity than catalyst **4a** in the asymmetric epoxidation of indene (conversion >99% vs 80.5%; ee, >99% vs 94.5%; entries 3 and 2). This was due to the high symmetry of rigid *p*-phenylenediamine which decreased the steric obstacles. For catalyst **4c**, a lower activity (conversion 86.4% vs >99%; ee, 92.3% vs >99%; entries 3 and 4) was displayed due to the bulkier linker benzidine making the substrates approach the catalyst with difficultly. For catalysts **4**(**d–g**), the catalytic activities increased with the length of the linkage in *m*-CPBA/NMO (entries 9–12). For instance, the ee values increased from 81% to 98%, conversion from 80% to >99% with the increase of carbon number of the alkyl diamine in the asymmetric epoxidation of indene, which was reported by Li's group [17] and our group [29]. The phenomenon can be interpreted as that the augmentation of the linkage was in favour of the heterogeneous salen Mn(III) complexes approaching the active intermediates of salen Mn(V) or their transition states more easily.

For $NaIO_4$/imidazole, neither the rigid aryl diamine nor the increase of the flexible chain length have effects on the catalytic activity. For example, the conversion and enantioselectivity exceed 99% (entries 19–21 and 25–28), which remained unchanged with the different linkers. This could be due to the superior oxidation of $NaIO_4$ so that the effect of the linkers on the catalytic ability can be neglected.

3.2.3. *Effect of the axial ligand*

Notably, high catalytic activities were obtained with the heterogeneous catalyst **4b** (conversion >99% vs 7.8%; ee, >99% vs 4.5%; entries 3 and 5) and the homogeneous catalyst **6a** (conversion 98.7% vs 91.2%; ee, 83.7% vs 25.5%; entries 7 and 8) in the absence of the additive NMO which is commonly required to improve the catalytic activity. This was in contrast to most literature reports [36]. Several factors contributed to this. First, the spatial orientation of the rigid aryl diamine can play the role of the *N*-oxide ligand (NMO). At the same time, the additives were generally axial ligands on the transition metal catalyst, which made the catalyst active either toward oxidation or toward reactivity with the olefin. When the *N*-oxide ligand (NMO) was added, a steric hindrance was brought about, and the optimal geometric configuration of the reactive intermediate salen Mn(V)=O was altered. The steric hindrance would prevent the olefins from approaching salen Mn (V)=O so that lower ee values were generated. However, the catalytic activity of catalyst **4g** (conversion >99% vs 51%; ee, 98% vs 8%; entries 12 and 13) and the homogeneous catalyst **6b** (conversion 89% vs 76%; ee, 86.7% vs 82.5%; entries 15 and 16) obviously increased with the addition of NMO in the epoxidation of indene, which was in agreement with most papers [25–27]. In summary, superior activity for the catalysts with rigid aryl diamines in the absence of NMO and for the catalysts with flexible alkyl diamines in the presence of NMO was observed.

For $NaIO_4$/imidazole, the superior catalytic activity of catalysts **4b** and **4g** as well as the homogeneous catalyst **6a** was still be maintained with the addition of imidazole and without (conversion up to 99%; ee%, up to 99%; entry 20 vs entry 22, entry 23 vs entry 24, entry 28 vs entry 29). For the homogeneous catalyst **6b,** the catalytic activity increased a little in the presence of imidazole (conversion 86% vs 83%; ee, 82% vs 79%; entry 30 vs entry 31). That was, the axial ligand imidazole had a subtle impact on the catalytic activity. The catalytic tests indicated excellent catalytic activities (conversion 97%; ee, >99%) in the absence of the axial ligand imidazole and lower activities (conversion 70%; ee, 88%) [37] with the addition of imidazole. Therefore, the additive imidazole played different roles in different catalyst systems.

3.3. *Reusability of the catalysts*

The reusability of a heterogeneous catalyst was of great importance from synthetic and economical points of view. Homogeneous catalysts usually cannot be recovered even once. However, supported catalysts **4(a–g)** could be filtered and reused several times with the retention of their activity.

As shown in Fig. 8, catalysts **4b** and **4g** maintained favourable activities after recycling nine times (conversion 88% vs 89%; ee, 86.1% vs 91%; **4b** and **4g**). The effective separating of the chiral salen Mn(III) complexes by the solid support ZnPS-PVPA could avoid the generation of the inactive μ-oxo-Mn(IV) species and ultimately contributed to the superior stability of the catalyst. The decrease of the yield was attributed to the decomposition of the chiral Mn(III) salen complex under epoxidative conditions [38] and the loss of hyperfine granules of the heterogeneous chiral Mn(III) salen catalyst. After recycling nine times, the Mn content of the catalysts **4b** and **4g** decreased (**4b**, 0.46 mmol/g; **4g**, 0.45 mmol/g) compared with the fresh catalyst (**4b**, 0.72 mmol/g; **4g**, 0.73 mmol/g). In the FT-IR spectra of the recovered catalyst **4b** (Fig. 9), the characteristic bands at 2954, 2864 and 1630 cm^{-1} disappeared or were weakened after recycling ten times, which indicated that the active sites of the salen Mn(III) complex and the support ZnPS-PVPA were partly destroyed under the acid reaction conditions.

3.4. *Large scale asymmetric epoxidation reaction*

We further carried out different scales of large scale asym-

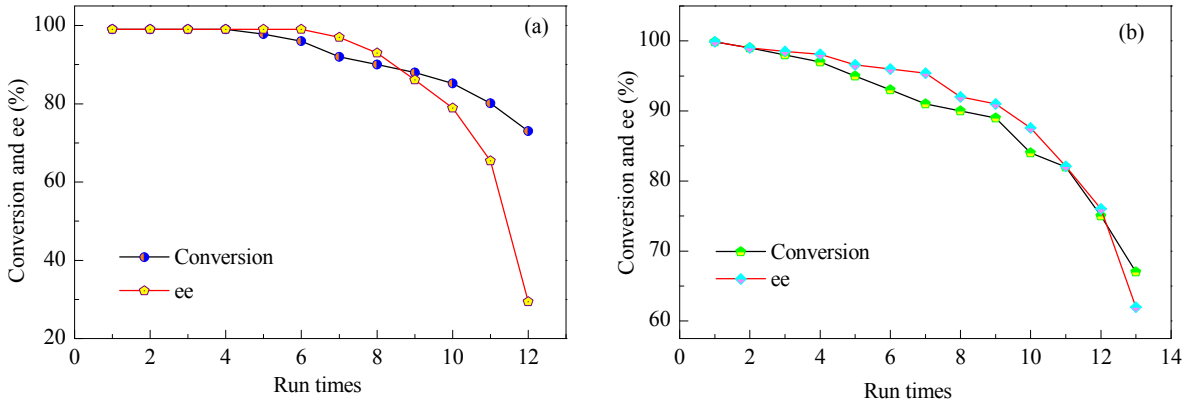

Fig. 8. Recycle of (a) catalysts **4b** and (b) catalyst **4g** in the asymmetric epoxidation of α-methylstyrene.

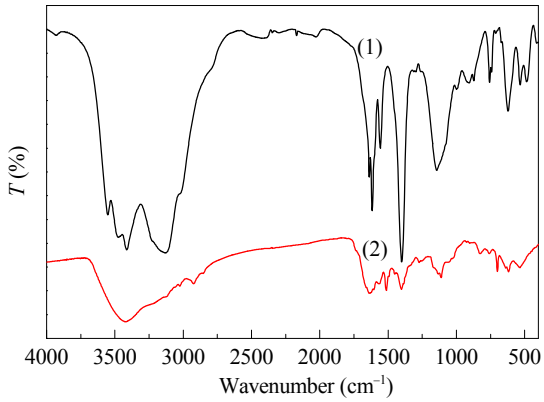

Fig. 9. FT-IR spectra of (1) fresh catalyst **4b** and (2) used catalyst **4b** used ten times.

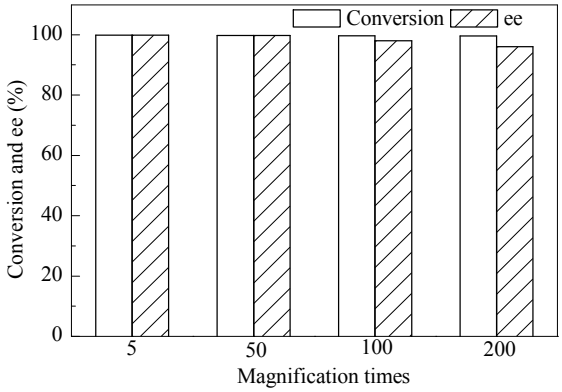

Fig. 10. Large scale asymmetric epoxidation reaction of α-methylstyrene.

metric epoxidation reactions with α-methylstyrene as substrate and *m*-CPBA as oxidant. The same catalyst loading of 5 mol% as that used in the experimental scale was employed. The large scale experiments could be facilely performed using the same procedure as the experimental scale reactions. The catalytic activities were shown in Fig. 10. Delightfully, the superior catalytic performance could still be maintained for the large scale reactions even when the scale was 200 times that of the experimental scale.

4. Conclusions

The epoxidation catalyst, Jacobsen's catalyst, anchored on ZnPS-PVPA gave good to excellent chemical yields and enantioselectivity in the asymmetric epoxidation of unfunctionalized alkenes. The heterogeneous catalyst retained its high atom efficiency after recycling nine times and could perform effectively on a large scale. The additives played different roles in different oxidation systems. However, the asymmetric induction was low in some cases. Further optimization and investigation of the scope and mechanisms of supported Jacobsen's catalyst for asymmetric epoxidation of alkenes are ongoing in our laboratory.

References

[1] H. C. Kolb, M. G. Finn, K. B. Sharpless, *Angew. Chem. Int. Ed.*, **2001**, 40, 2004–2021.
[2] R. V. Ottenbacher, K. P. Bryliakov, E. P. Talsi, *Adv. Synth. Catal.*, **2011**, 353, 885–889.
[3] S. H. Liao, B. List, *Angew. Chem. Int. Ed.*, **2010**, 49, 628–631.
[4] S. Mayer, B. List, *Angew. Chem. Int. Ed.*, **2006**, 45, 4193–4195.
[5] N. J. A. Martin, B. List, *J. Am. Chem. Soc.*, **2006**, 128, 13368–13369.
[6] J. Seayad, B. List, *Org. Biomol. Chem.*, **2005**, 3, 719–724.
[7] F. Rosati, G. Roelfes, *ChemCatChem*, **2010**, 2, 916–927.
[8] P. Goodrich, C. Hardacre, C. Paun, A. Ribeiro, S. Kennedy, M. J. V. Lourenco, H. Manyar, C. A. Nieto de Castro, M. Besnea, V. I. Pârvulescu, *Adv. Synth. Catal.*, **2011**, 353, 995–1004.
[9] A. Kuschel, M. Luka, M. Wessig, M. Drescher, M. Fonin, G. Kiliani, S. Polarz, *Adv. Funct. Mater.*, **2010**, 20, 1133–1143.
[10] S. L. Wei, Y. H. Tang, X. Q. Xu, G. J. Xu, Y. Yu, Y. Sun, Y. S. Zheng, *Appl. Organometal. Chem.*, **2011**, 25, 146–153.
[11] T. Punniyamurthy, S. Velusamy, J. Iqbal, *Chem. Rev.*, **2005**, 105, 2329–2364.
[12] E. M. McGarrigle, D. G. Gilheany, *Chem. Rev.*, **2005**, 105, 1563–1602.
[13] E. N. Jacobsen, W. Zhang, M. L. Guler, *J. Am. Chem. Soc.*, **1991**, 113, 6703–6704.
[14] V. La. Paglia. Fragola, F. Lupo, A. Pappalardo, G. Trusso. Sfrazzetto, R. M. Toscano, F. P. Ballistreri, G. A. Tomaselli, A. Gulino, *J. Mater. Chem.*, **2012**, 22, 20561–20565.
[15] I. Kuzniarska. Biernacka, C. Pereira, A. P. Carvalho, J. Pires, C.

Graphical Abstract

Chin. J. Catal., 2016, 37: 1539–1548 doi: 10.1016/S1872-2067(16)62489-0

Enantioselective epoxidation of unfunctionalized olefins by Jacobsen's catalyst immobilized on amino-modified ZnPS-PVPA

Jing Huang*, Yan luo, Jiali Cai
Xihua University; Southwest University; Chongqing University of Arts and Science

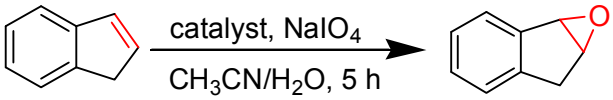

The recyclable catalysts immobilized salen Mn(III) onto ZnPS-PVPA upon diamines displayed superior catalytic ability both for experimental scale and for large-scale reactions.

Freire, *Appl. Clay Sci.*, **2011**, 53, 195–203.
[16] Z. R. Zhang, F. Guan, X. W. Huang, Y. D. Wang, Y. Sun, *J. Mol. Catal. A*, **2012**, 363–364, 343–353.
[17] H. Zhang, Y. Zhang, C. Li, *J. Catal.*, **2006**, 238, 369–381.
[18] T. Roy, R. I. Kureshy, N. H. Khan, S. H. R. Abdi, A. Sadhukhan, H. C. Bajaj, *Tetrahedron*, **2012**, 68, 6314–6322.
[19] P. K. Bera, N. C. Maity, S. H. R. Abdi, N. H. Khan, R. I. Kureshy, H. C. Bajaj, *Appl. Catal. A*, **2013**, 467, 542–551.
[20] Y. J. Chen, R. Tan, Y. Y. Zhang, G. W. Zhao, W. G. Zheng, R. C. Luo, D. H. Yin, *Appl. Catal. A*, **2015**, 491, 106–115.
[21] M. Liu, Z. P. Zhao, K. C. Chen, W. F. Liu, *Catal. Commun.*, **2015**, 64, 70–74.
[22] R. N. Ji, K. Yu, L. L. Lou, S. X. Liu, *J. Mol. Catal. A*, **2013**, 378, 7–16.
[23] G. J. Xu, S. L. Wei, Y. G. Fan, L. B. Zhu, Y. H. Tang, Y. S. Zheng, *Chin. J. Catal.*, **2012**, 33, 473–477.
[24] F. A. Almeida Paz, J. Klinowski, S. M. F. Vilela, J. P. C. Tomé, J. A. S. Cavaleiroc, J. Rocha, *Chem. Soc. Rev.*, **2012**, 41, 1088–1110.
[25] W. S. Ren, X. K. Fu, H. B. Bao, R. F. Bai, P. P. Ding, B. L. Sui, *Catal. Commun.*, **2009**, 10, 788–793.
[26] X. B. Tu, X. K. Fu, Hu, X. Y. Hu, Y. D. Li, *Inorg. Chem. Commun.*, **2010**,13, 404–407.
[27] B. W. Gong, X. K. Fu, J. X. Chen, Y. D. Li, X. C. Zou, X. B. Tu, P. P. Ding, L. P. Ma, *J. Catal.*, **2009**, 262, 9–17.
[28] J. Huang, X. K. Fu, G. Wang, C. Li, X. Y. Hu, *Dalton Trans.*, **2011**, 40, 3631–3639.
[29] J. Huang, X. K. Fu, G. Wang, Q. Miao, G. M. Wang, *Dalton Trans.*, **2012**, 41, 10661–10669.
[30] J. Huang, X. K. Fu, Q. Miao, *Appl. Catal. A*, **2011**, 407, 163–172.
[31] J. Huang, X. K. Fu, Q. Miao, *Catal. Sci. Technol.*, **2011**, 1, 1472–1482.
[32] J. Huang, M. Tang, X. Li, G. Z. Zhong, C. M. Li, *Dalton Trans.*, **2014**, 43, 17500–17508.
[33] W. Zhang, J. L. Loebach, S. R. Wilson, E. N. Jacobsen, *J. Am. Chem. Soc.*, **1990**, 112, 2801–2803.
[34] W. Zhang, N. H. Lee, E. N. Jacobsen, *J. Am. Chem. Soc.*, **1994**, 116, 425–426.
[35] B. W. Gong, X. K. Fu, H. S. Shen, L. H. Ma, Y. J. Xia, *Fine Chem.*, **2008**, 25, 603–605.
[36] C. Li, *Catal. Rev. Sci. Eng.*, **2004**, 46, 419–492.
[37] X. Y. Hu, X. K. Fu, J. W. Xu, C. W. Wang, *J. Organomet. Chem.*, **2011**, 696, 2797–2804.
[38] C. E. Song, E. J. Roh, B. M. Yu, D. Y. Chi, S. C. Kim, K. J. Lee, *Chem. Commun.*, **2000**, 7, 615–616.

Page numbers refer to the contents in the print version, which include both the English version and extended Chinese abstract of the paper. The online version only has the English version. The pages with the extended Chinese abstract are only available in the print version.